Journal of Power Sources 184 (2008) 494–497

Contents lists available at ScienceDirect

Journal of Power Sources

journal homepage: www.elsevier.com/locate/jpowsour

Short communication

Low-temperature synthesis of highly crystallized $LiMn_2O_4$ from alpha manganese dioxide nanorods☆

Haisheng Fang, Liping Li, Yong Yang, Guofeng Yan, Guangshe Li*

State Key Lab of Structural Chemistry, Fujian Institute of Research on the Structure of Matter and Graduate School of Chinese Academy of Sciences, Fuzhou 350002, PR China

ARTICLE INFO

Article history:
Received 20 December 2007
Received in revised form 7 April 2008
Accepted 7 April 2008
Available online 12 April 2008

Keywords:
Lithium ion battery
Cathode
$LiMn_2O_4$
α-MnO_2
Nanorod

ABSTRACT

One-dimensional alpha manganese dioxide (α-MnO_2) nanorods synthesized by a hydrothermal route were explored as the starting material for preparing lithium manganese spinel $LiMn_2O_4$. Pure and highly crystalline spinel $LiMn_2O_4$ was easily obtained from α-MnO_2 nanorods through a low-temperature solid-state reaction route, while Mn_2O_3 impurity was present along with the spinel phase when commercial MnO_2 was used as starting material. The particle size of $LiMn_2O_4$ prepared from α-MnO_2 nanorods was about 100 nm with a homogenous distribution. Electrochemical tests demonstrated that the $LiMn_2O_4$ thus prepared exhibited a higher capacity than that prepared from commercial MnO_2. Therefore, α-MnO_2 nanorods are proved to be a promising starting material for the preparation of high quality $LiMn_2O_4$.

1. Introduction

Lithium ion batteries are widely used in electronic devices, hybrid electric vehicles, portable power tools and many power supplies due to their high energy and power density. $LiCoO_2$ is the currently commercially used cathode material for lithium ion batteries, and has a good electrochemical performance. However, the high cost and toxicity of cobalt have always been a big problem. As a result, intensive efforts have been performed to search for alternative cathode materials [1–4]. Spinel $LiMn_2O_4$ is a promising cathode material for lithium ion batteries due to its low cost, environmental friendliness and good safety, in spite of some disadvantages like small capacity and low stability at high temperatures [1,3–5].

Generally, the electrochemical performance of electrode materials is closely associated with the phase crystallinity, purity, particle size and distribution. These important factors depend strongly on the preparation methods [3]. The traditional solid-state reaction method was often used to produce single phase $LiMn_2O_4$, but it requires prolonged high temperature calcination (800 °C) owing to the low reactivity of the starting materials [3,6,7], which causes an inevitable coarsening of the powders with a broad size distribution and an oxygen deficiency, ultimately impairing the electrochemical properties of $LiMn_2O_4$ [8]. As a result, a number of soft chemistry techniques have been explored to prepare $LiMn_2O_4$, such as sol–gel [9,10], Pechini process [11,12], combustion [13,14], and polymer precursor method [15]. Although uniform $LiMn_2O_4$ particles with good electrochemical performance could be thus obtained, the synthetic procedures are generally complex. Therefore, a simple and convenient route to synthesize $LiMn_2O_4$ without loss of electrochemical performance is highly desired. From various synthetic methods reported in the previous literatures, the results clearly indicated that the preparation conditions including reaction temperature and time, and the physicochemical properties of the resulting product including structure, purity, morphology, and electrochemical performance are greatly influenced by the precursor or starting materials [3,16,17]. Thus, a proper choose of starting materials is very important for the preparation of high performance cathode materials for lithium ion batteries.

α-MnO_2 was reported to have a special one-dimensional tunnel structure with a good absorption property [18,19], which is thus expected to be helpful for the incorporation of Li^+ into its structure and hence facilitating the formation of $LiMn_2O_4$ in the subsequent reaction. Furthermore, considering the high reactivity of nanoparticle due to its high surface area, the use of nanostructured MnO_2 as starting material may accelerate the formation of $LiMn_2O_4$ at a reduced calcination temperature. In virtue of these advantages, it is highly expected that nanostructured α-MnO_2 would be a superior starting material for low-temperature synthesis of $LiMn_2O_4$. Among various nanostructures, one-dimensional

☆ The manuscript is intended for the IBA 2007 special issue.

* Corresponding author. Tel.: +86 591 83702122; fax: +86 591 83714946.
E-mail address: guangshe@fjirsm.ac.cn (G. Li).

0378-7753/$ – see front matter © 2008 Elsevier B.V. All rights reserved.
doi:10.1016/j.jpowsour.2008.04.011

α-MnO_2 nanorods are more promising for our purpose, and have readily been synthesized [19–21], however, the application of α-MnO_2 nanorods as starting material for the preparation of $LiMn_2O_4$ still remains virgin to date.

In this work, we report on the synthesis of $LiMn_2O_4$ using α-MnO_2 nanorods as the starting material which were obtained by a hydrothermal route. It is found that pure and well-crystallized $LiMn_2O_4$ with an improved capacity was prepared by a simple solid-state reaction at a relatively low temperature of 600 °C in a short period of time of 4 h.

2. Experimental

All chemicals were of analytical grade and used without further purification. α-MnO_2 nanorods were prepared according to a procedure as reported elsewhere [19]. The synthesis process could be briefly described as follow: $(NH_4)_2S_2O_8$, $MnSO_4{\cdot}H_2O$ and $(NH_4)_2SO_4$ with a molar ratio of 1:1:5 were fully mixed in 30 mL distilled water by ultrasonication and magnetic stirring to form a homogeneous suspension at room temperature, which was then transferred into a Teflon-lined stainless steel autoclave and heated at 160 °C for 12 h. A reaction during the heating process could be described as below:

$$MnSO_4 + (NH_4)_2S_2O_8 + 2H_2O \rightarrow MnO_2 + (NH_4)_2SO_4 + 2H_2SO_4 \quad (1)$$

The precipitated product was collected after the reaction, washed repeatedly with distilled water, and finally dried at 120 °C.

In a typical synthesis of $LiMn_2O_4$, appropriate amounts of $LiCH_3COO{\cdot}6H_2O$ (0.612 g) was dissolved into 30 mL distilled water. Subsequently, the as-prepared α-MnO_2 nanorods (0.869 g) were added into the solution, and vigorously stirred for several hours at room temperature. The resulting slurry was dried in air at 80 °C, and then calcined at 600 °C in air for 4 h with an intermediate manual grinding. For comparison, commercial MnO_2 (particle size: 3–5 μm) was also used as a starting material to prepare $LiMn_2O_4$ via the same route.

Thermogravimetric and differential thermal analysis (TG/DTA) of the precursor was performed with a TA instruments (Netzsch thermoanalyzer STA449C) at a heating rate of 15 °C min^{-1} in a constant flow of extra dry air. Powder X-ray diffraction (XRD) patterns of the products were recorded on apparatus (DMAX2500, Rigaku, Japan) at room temperature using Cu Kα radiation to identify the crystalline phase. Fourier transform infrared spectrum (FTIR) of the product was carried out with a PerkinElmer IR spectrophotometer using KBr pellet technique. The size and morphology of the products were observed by a scanning electron microscopy (SEM, JEOL, JSM6700F, Japan). The surface area of α-MnO_2 nanorods was determined by Brunauer–Emmett–Teller method (BET, ASAP2020, Micromeritics Inc.) with nitrogen as adsorption gas.

Electrochemical characterizations of the product were performed using CR2025 coin-type cell. For cathode fabrication, the as-prepared powders were mixed with 10 wt.% of carbon black and 10 wt.% of polyvinylidene fluoride in *N*-methyl pyrrolidinone until a slurry was formed. Then, the blended slurries were pasted onto an aluminum current collector, and the electrode was dried at 100 °C for 10 h in vacuum. The test cell consisted of the cathode and lithium foil anode which were separated by a porous polypropylene film and electrolyte of 1 M $LiPF_6$ in ethylene carbonate (EC)/ethyl methyl carbonate (EMC)/dimethyl carbonate (DMC) (1:1:1 in volume). The assembly of the cells was carried out in a dry Ar-filled glove box. The cells were charged and discharged over a voltage range of 3–4.5 V versus Li^+/Li electrode at room temperature. Cyclic voltammograms (CVs) were measured on a CHI660C electrochemistry workstation (Chenhua, Shanghai, China) with a scan rate of 0.05 mV s^{-1} between 3.0 and 4.5 V versus Li^+/Li.

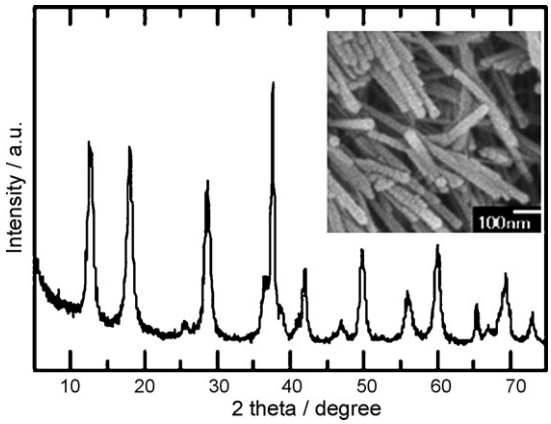

Fig. 1. X-ray diffraction pattern and SEM image (inset) of the as-prepared α-MnO_2 nanorods.

3. Results and discussion

As can be seen from the reaction (1), the formation reaction of α-MnO_2 nanorods is quite simple: no catalyst or organic template is needed. All involved chemicals are of low cost and low toxicity, and the procedures in the synthesis are facile to manipulate, thus large-scale production of α-MnO_2 nanorods for practical application is possible. Fig. 1 shows the XRD pattern of the prepared MnO_2. All diffraction peaks can be fully indexed into a tetragonal structure with a space group of *I*4/*m*, indicating the formation of a single α-MnO_2 phase with lattice parameters $a = 9.7847$, $c = 2.8630$ Å (JCPDS 44-0141). The broadened diffraction peaks indicate the small size of the obtained α-MnO_2. The inset of Fig. 1 shows the SEM image of the prepared α-MnO_2. Nanorods were clearly observed throughout the sample. Most of the rods are several tens of nanometers in diameter. The surface area of the prepared α-MnO_2 nanorods estimated by BET method was 108 m^2 g^{-1}. Such a high surface area of α-MnO_2 nanorods allows to achieve large contact with lithium salt in the subsequent solid-state reaction, and thereby, to accelerate the formation process of $LiMn_2O_4$. This assumption was directly evidenced by the thermal evolution of the precursor, as the TG/DTA curves in Fig. 2 clearly indicated that the reaction temperature could be remarkably reduced when α-MnO_2 nanorods were used.

Fig. 3 shows X-ray diffraction pattern of the sample prepared from α-MnO_2 nanorods. For comparison, XRD pattern of the sam-

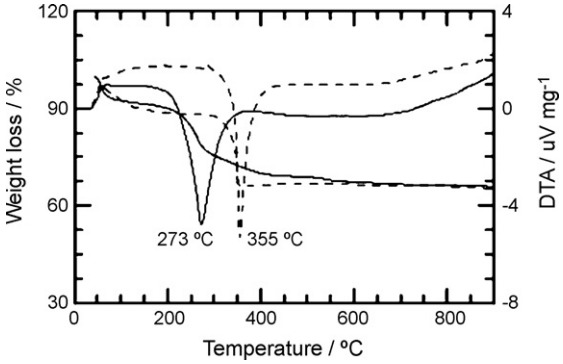

Fig. 2. TG/DTA curves of the precursor using α-MnO_2 nanorods (solid line) and commercial MnO_2 (dashed line).

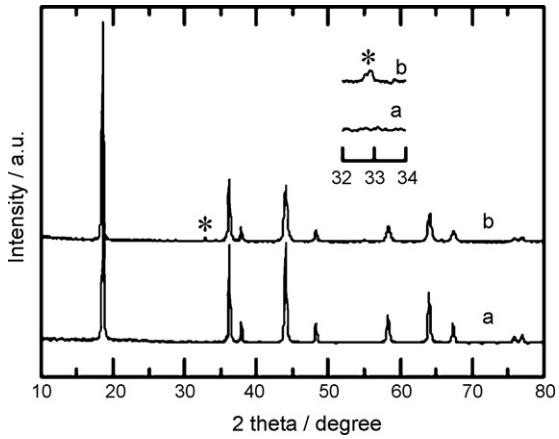

Fig. 3. X-ray diffraction patterns of the $LiMn_2O_4$ prepared from (a) α-MnO_2 nanorods and (b) commercial MnO_2. The asterisk indicates the impurity Mn_2O_3.

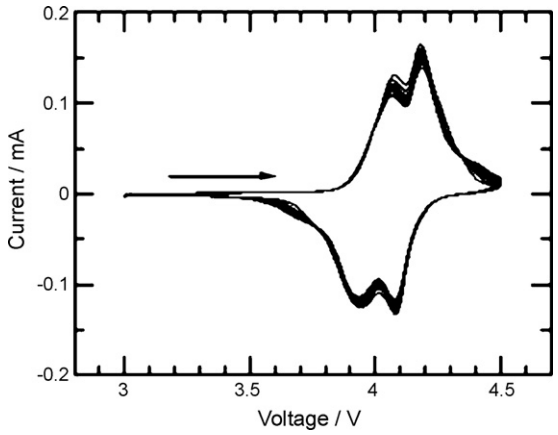

Fig. 5. Cyclic voltammograms of the $LiMn_2O_4$ prepared from α-MnO_2 nanorods within the voltage range from 3.0 to 4.5 V versus Li/Li^+ at a scan rate of 0.05 mV s^{-1}.

ple prepared from commercial MnO_2 was also shown in Fig. 3. For the sample prepared from α-MnO_2 nanorods, all diffraction peaks can be fully assigned to a cubic spinel structure with a space group of *Fd*3*m* (Fig. 3a), demonstrating the formation of a single $LiMn_2O_4$ spinel. The strong and sharp XRD peaks indicate the high crystallinity of the obtained $LiMn_2O_4$ powders. For the sample prepared from commercial MnO_2, however, Mn_2O_3 impurity was present in the final product (Fig. 3b), indicating the incompleteness of solid-state reaction likely due to the low reactivity of commercial MnO_2. In addition, the broadened and relatively weak diffraction peaks indicated the low crystallinity of the obtained $LiMn_2O_4$. Fig. 4 shows IR spectrum of the sample prepared from α-MnO_2 nanorods. The spectrum exhibits two strong absorbance peaks in the range 400–700 cm^{-1}, which are the IR features of spinel $LiMn_2O_4$ [22]. These results strongly suggest that the use of α-MnO_2 nanorods as starting material may favor the preparation of high purity and highly crystalline $LiMn_2O_4$ spinel at relatively low temperature. It is clear that the reduced sintering temperature reported in this work benefited from the high reactivity of α-MnO_2 nanorods. The inset of Fig. 4 shows the SEM image of the $LiMn_2O_4$ prepared from α-MnO_2 nanorods. It is seen that the average particle size was about 100 nm with a fairly narrow particle size distribution. Thus, the α-MnO_2 nanorods could easily react with lithium salt to produce pure, fine, and homogenous $LiMn_2O_4$ powders.

In spinel $LiMn_2O_4$, Li^+ ions occupy the tetrahedral sites (8a), while Mn^{3+} and Mn^{4+} ions reside in the octahedral sites (16d), and O^{2-} ions are located in 32e sites [3]. The oxygen ions form a cubic closely packed array, tetrahedral sites (8a) share faces with vacant octahedral sites (16c), and thus form a three-dimensional vacant channel. Lithium ions can reversibly intercalate or de-intercalate through these channels during the electrochemical reaction. This process was monitored by a cyclic voltammetry. Fig. 5 shows several continuous cyclic voltammograms for $LiMn_2O_4$ prepared from α-MnO_2 nanorods with the voltage range from 3.0 to 4.5 V versus Li/Li^+ at a scan rate of 0.05 mV s^{-1}. Two couples of reversible redox peaks are observed in the CV curves. These peaks illustrate well the reversible electrochemical deinsertion/insertion of Li^+ from/into the tetrahedral sites of $LiMn_2O_4$, while keeping a good stability with cycling. The split of the redox peaks into two couples shows that the electrochemical reaction of the extraction and insertion of lithium ions occurred in two stages [23,24]. The first oxidation peak is ascribed to the removal of Li^+ from half of the tetrahedral sites in which Li–Li interactions exist, whereas the second oxidation peak is attributed to the removal of Li^+ from the remaining tetrahedral sites where no Li–Li interactions exist. The whole process can be described as follows [25]:

$$0.5Li^+ + 0.5e + 2\lambda\text{-}MnO_2 \Leftrightarrow Li_{0.5}Mn_2O_4 \quad (2)$$

$$0.5Li^+ + 0.5e + Li_{0.5}Mn_2O_4 \Leftrightarrow LiMn_2O_4 \quad (3)$$

Electrochemical properties of the obtained $LiMn_2O_4$ are preliminarily evaluated using 2025 coin-type cell. Representative charge–discharge curves of the obtained $LiMn_2O_4$ are shown in Fig. 6a. The cells were cycled at a current density of 20 mA g^{-1}

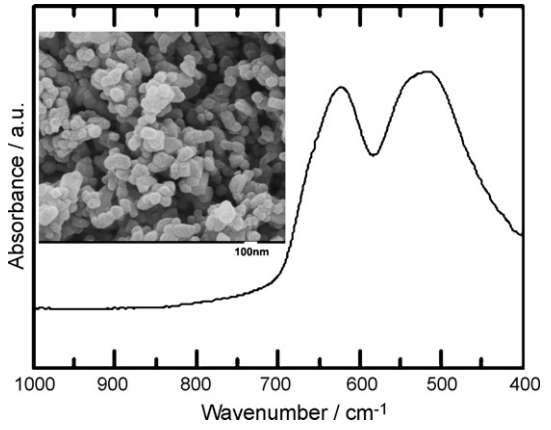

Fig. 4. FTIR spectrum and SEM image (inset) of $LiMn_2O_4$ prepared from α-MnO_2 nanorods.

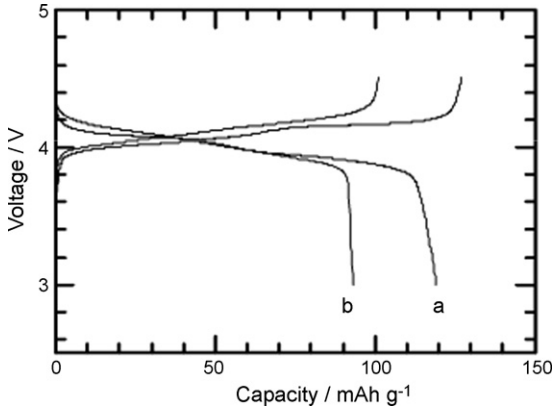

Fig. 6. Charge/discharge curves of the $LiMn_2O_4$ prepared from (a) α-MnO_2 nanorods and (b) commercial MnO_2 in the voltage range from 3.0 to 4.5 V versus Li/Li^+ at a current density of 20 mA g^{-1}.

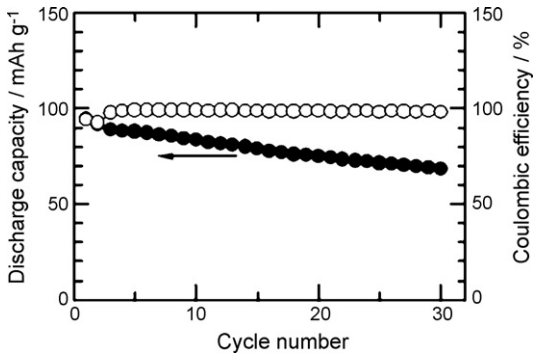

Fig. 7. Discharge capacity and Coulombic efficiency versus cycle number of the $LiMn_2O_4$ prepared from α-MnO_2 nanorods. The cycling was performed in the voltage range from 3.0 to 4.5 V versus Li/Li^+ at a high current density of 240 mA g^{-1}.

between 3 and 4.5 V. The charge–discharge curves exhibited two close pseudo plateaus at around 4.0 V, which is a typical profile for the electrochemical extraction and insertion of lithium ion. This result confirms two equilibrium binary systems during Li^+ intercalation, i.e., λ-MnO_2–$Li_{0.5}Mn_2O_4$ and $Li_{0.5}Mn_2O_4$–$LiMn_2O_4$ [26], and is perfectly consistent with what was observed in Fig. 5. Meanwhile, it is noted that the $LiMn_2O_4$ synthesized from α-MnO_2 nanorods showed a much higher capacity than that prepared from commercial MnO_2. When cycled at a current density of 20 mA g^{-1}, a reversible capacity of 120 mAh g^{-1} was observed for $LiMn_2O_4$ synthesized from α-MnO_2 nanorods (Fig. 6a), while only a capacity <95 mAh g^{-1} was observed for that prepared from commercial MnO_2 (Fig. 6b). This is in accordance with the previous results [16,27,28] in which the presence of impurities and low crystallinity of electrode materials limited the available capacity. Moreover, the $LiMn_2O_4$ synthesized from α-MnO_2 nanorods also showed a good electrochemical performance at high rates (Fig. 7). Consequently, the starting materials could play a key role in determining the electrochemical performance of $LiMn_2O_4$. From the above results, α-MnO_2 nanorods are proved to be a quite promising starting material for the preparation of highly crystallized and high performance $LiMn_2O_4$.

4. Conclusions

Using α-MnO_2 nanorods as a starting material, pure and highly crystallized $LiMn_2O_4$ was easily obtained via a low-temperature reaction in a short time (600 °C, 4 h). The electrochemical performance measurements showed that the $LiMn_2O_4$ obtained from α-MnO_2 nanorods had a significantly improved capacity in comparison with that prepared from commercial MnO_2. These results demonstrate that α-MnO_2 nanorods are an excellent starting material for the synthesis of cubic $LiMn_2O_4$ spinel.

Acknowledgements

This work was financially supported by the Knowledge Innovation Program of the Chinese Academy of Sciences, NSFC under the contract (no. 20671092, 20773132, 20771101), Science and Technology Program from Fujian Province (no. 2006H0040), Directional program (no. KJCX-YW-M05), 973 project (no. 2007CB613301) and FJIRSM project (no. SZD08002-3). Authors express their thanks to Mr. Yingzhen Pan for providing the starting materials of α-MnO_2 nanorods.

References

[1] J.M. Tarascon, M. Armand, Nature 414 (2001) 359.
[2] E. Antolini, Solid State Ionics 170 (2004) 159.
[3] G. Amatucci, J.M. Tarascon, J. Electrochem. Soc. 149 (2002) K31.
[4] M.M. Thackeray, C.S. Johnson, J.T. Vaughey, N. Li, S.A. Hackney, J. Mater. Chem. 15 (2005) 2257.
[5] M.M. Thackeray, W.I.E. David, P.G. Bruce, J.B. Goodenough, Mater. Res. Bull. 18 (1983) 461.
[6] J. Guan, M. Liu, Solid State Ionics 110 (1998) 21.
[7] G. Li, A. Yamada, Y. Fukishima, K. Yamaura, T. Saito, T. Endo, H. Azuma, K. Sekai, Y. Nishi, Solid State Ionics 130 (2000) 221.
[8] Y.G. Xia, H.Y. Wang, Q. Zhang, H. Nakamura, H. Noguchi, M. Yoshio, J. Power Sources 166 (2007) 485.
[9] C.J. Curtis, J.X. Wang, D.L. Schulz, J. Electrochem. Soc. 151 (2004) A590.
[10] J.H. Choy, D.H. Kim, C.W. Kwon, S.J. Hwang, Y.I. Kim, J. Power Sources 77 (1999) 1.
[11] W. Liu, G.C. Farrington, F. Chaput, B. Dunn, J. Electrochem. Soc. 143 (1996) 879.
[12] D. Song, H. Ikuta, T. Uchida, M. Wakihara, Solid State Ionics 117 (1999) 151.
[13] W.S. Yang, G. Zhang, J.Y. Xie, L.L. Yang, Q.G. Liu, J. Power Sources 80–82 (1999) 412.
[14] D. Kovacheva, H. Gadjov, K. Petrov, S. Mandal, M.G. Lazarraga, L. Pascual, J.M. Amarilla, R.M. Rojas, P. Herrero, J.M. Rojo, J. Mater. Chem. 12 (2002) 1184.
[15] A. Subramania, N. Angayarkanni, N. Niruba, T. Vasudevan, Nanotechnology 18 (2007) 065603.
[16] Y.M. Hon, K.Z. Fung, S.P. Lin, M.H. Hon, J. Solid State Chem. 163 (2002) 231.
[17] S.J. Bao, C.M. Li, H.L. Li, J.H.T. Luong, J. Power Sources 164 (2007) 885.
[18] M.M. Thackeray, Prog. Solid State Chem. 25 (1997) 1.
[19] X. Wang, Y.D. Li, J. Am. Chem. Soc. 124 (2002) 2880.
[20] F.Y. Cheng, J.Z. Zhao, W. Song, C.S. Li, H. Ma, J. Chen, P.W. Shen, Inorg. Chem. 45 (2006) 2038.
[21] H.E. Wang, Z.G. Lu, D. Qian, Y.J. Li, W. Zhang, Nanotechnology 18 (2007) 115616.
[22] B. Ammundsen, G.R. Burns, M.S. Islam, H. Kanoh, J. Roziére, J. Phys. Chem. B 103 (1999) 5175.
[23] Y.Y. Xia, M. Yoshio, J. Electrochem. Soc. 143 (1996) 825.
[24] A. Ott, P. Endres, V. Klein, B. Fuchs, A. Jager, H.A. Mayer, S. Kemmler-Sack, H.W. Praas, K. Brandt, G. Filoti, V. Kunczer, M. Rosenberg, J. Power Sources 72 (1998) 1.
[25] M. Armand, F. Dalard, D. Reroo, C. Mouliom, Solid State Ionics 15 (1985) 205.
[26] Y.K. Sun, K.H. Lee, S.I. Moon, I.H. Oh, Solid State Ionics 112 (1998) 237.
[27] A. Manthiram, J. Kim, Chem. Mater. 10 (1998) 2895.
[28] J.C. Arrebola, A. Caballero, M. Cruz, L. Hernan, J. Morales, E.R. Castellon, Adv. Funct. Mater. 16 (2006) 1904.